CHAPTER 7

SUMMARY AND CONCLUSIONS

7.1 SUMMARY

This thesis presents some new optical configurations in speckle interferometry for in-plane and out-of-plane displacement measurements, depth contouring and slope contouring. This study is mainly focused on the development of new techniques for in-plane displacement measurements as they are widely used for other applications such as strain measurements, depth contouring and slope contouring etc. In Chapter 2, some of the problems faced from Leendertz's and Duffy's methods for measuring in-plane displacement have been solved. Leendertz's method measures very small displacements and decorrelate faster for larger displacements, whereas Duffy's method measures larger displacements but is insensitive to very small displacements. Therefore in order to know the displacement range for a given test object two different experiments have to be performed. This particular problem has been elegantly solved by combining both the techniques in a single experimental arrangement as shown in Figure 2.2. This arrangement generates two sets of fringes corresponding to the phase change $\vec{\delta}_L$ and $\vec{\delta}_D$ respectively. The fine fringes generated due to the phase change $\vec{\delta}_L$ are inside the coarse fringes generated due to the phase change $\vec{\delta}_D$. Here, if the displacement range is very small then the method generates a number of finer fringes and generates both coarse and finer fringes if the displacement range is higher. However, for large displacements the coarse

fringes are more visible and hence are taken into account for computation. This is the main advantage of this configuration. Figures 2.3(a) and (b) show the u-component of the in-plane displacement fringes of a circular diaphragm subjected to rigid body in-plane rotations of about 0.45 and 0.9 mrads, respectively. The close agreement between theory and experiment has been tested with computer simulated fringes shown in Figures 2.4(a) and (b) respectively. Fringes corresponding to the v-component of the in-plane displacement can be obtained when the illuminating beam and the two aperture mask lie in the y–z plane as shown in Figure 2.5 for a cantilever beam fixed at one end and loaded at the other end. The graph shown in Figure 2.6 verifies the validity of the method. The demerit of this configuration is that the visibility of the finer fringes seen on the bright coarse fringes is poor due to the high d.c. term which is evident from the irradiance profile shown in Figure 2.2.

The above mentioned problems are solved in the configuration developed in the present study shown in Figure 2.7. As the observed beams (scattered from the object) enter the image plane through each half of the imaging lens and combine only at the image plane the decorrelation sets in rather slowly. Therefore interference fringes are obtained even for quite a large amount of displacements with unit contrast. This configuration is well-suited for in-plane displacement measurements as the sensitivity can be varied very easily by just moving mirrors M_1 and M_2 (Figure 2.7) towards or away from mirrors M_3 and M_4, respectively. The main advantage of this configuration is that with a single beam illumination one can achieve a sensitivity which is realised for the first time and is equal to that of Leendertz's method. The aperture mask is not required in this set-up, however, it acts as a prefiltering arrangement and improves the contrast of the fringes. Further this configuration has been modified by introducing a beam splitter before the imaging lens in order to adopt this configuration in ESPI for real time measurements which is much more useful for industrial applications. However, in the modified configuration, it is interesting to note

that instead of a dual direction of observation, a single direction of observation does not contribute to fringe formation because the beams entering apertures A_1 and A_2 undergo identical phase changes on deformation and hence the net phase change is zero. It also allows simultaneous monitoring of the object at two different work stations. Both the configurations are tested by conducting experiments on several objects.

A new theoretical concept has been given to account for the two-fold increase in sensitivity for the measurement of in-plane displacement using the configuration proposed by Sirohi and Krishna Mohan (1993a). This method takes into account all the four beams entering apertures A_1 and A_2 for computing the net phase change. It is observed that the sensitivity is not increased when all the four beams are present for fringe formation whereas it is increased by two-fold only when the backscattered beams are present for fringe formation. Theoretical and experimental results have been presented to strengthen the concept. Table 7.1 presents all the configurations with their intensity distributions, irradiance profile and measuring sensitivity.

Since aperturing of the lens offers several advantages, we developed a three aperture speckle interferometric configuration for the simultaneous measurement of in-plane and out-of-plane displacements with comparable sensitivities. In this configuration the object is illuminated by two collimated beams. Of the three apertures one is used for generating a diffuse reference beam by mounting a small ground glass plate on it and the other two apertures are used for image formation. During whole-field filtering of the specklegram five diffraction halos are generated. The fringe pattern obtained through diffraction halo A_{12} directly yields the in-plane displacement component whereas the other halos yield both the in-plane and out-of-plane displacement components as a moiré pattern. Then the out-of-plane displacement component is separated through computation. The advantages of this technique is that the sensitivity of in-plane displacement measurement is enhanced due to the two beam illumination arrangement compared to the

Table 7.1 Various speckle interferometric configurations for the measurement of in-plane displacement

Optical configuration	Irradiance distribution and its profile	Sensitivity of the configuration (Δu
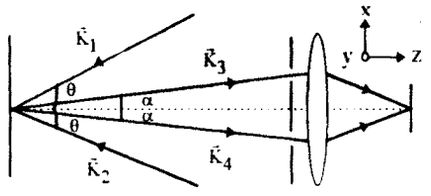	$c\{2+\cos(\vec{K}_4-\vec{K}_3)\cdot\vec{L}$ $[1+\cos(\vec{K}_2-\vec{K}_1)\cdot\vec{L}]\}$ 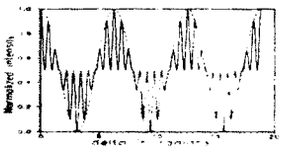	$\frac{\lambda}{2\sin\alpha}$ & $\frac{\lambda}{2\sin\theta}$
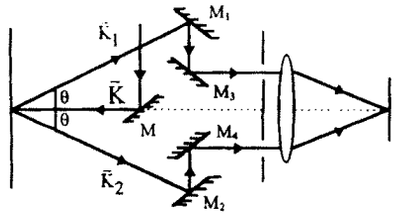	$c[1+\cos(\vec{K}_2-\vec{K}_1)\cdot\vec{L}]$ 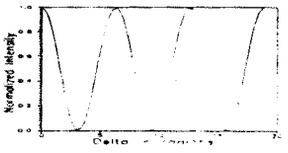	$\frac{\lambda}{2\sin\theta}$
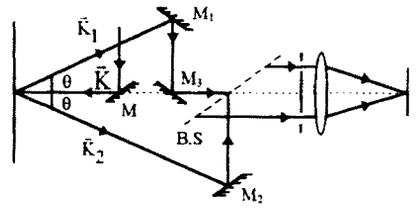	$c[1+\cos(\vec{K}_2-\vec{K}_1)\cdot\vec{L}]$ 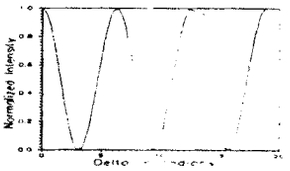	$\frac{\lambda}{2\sin\theta}$
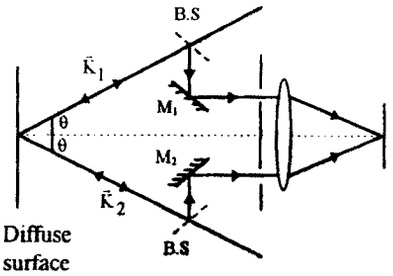 Diffuse surface	$c\{2+\cos(\vec{K}_2-\vec{K}_1)\cdot\vec{L}$ $[1+\cos(\vec{K}_2-\vec{K}_1)\cdot\vec{L}]\}$ 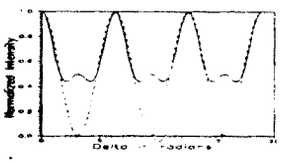	$\frac{\lambda}{2\sin\theta}$
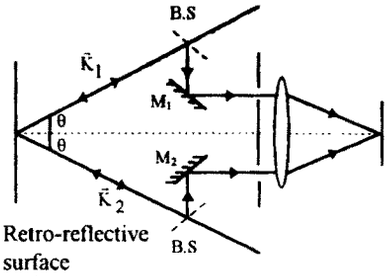 Retro-reflective surface	$c[1+\cos(2(\vec{K}_2-\vec{K}_1))\cdot\vec{L}]$ 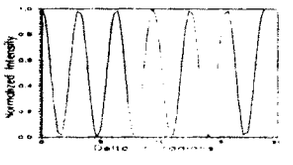	$\frac{\lambda}{4\sin\theta}$

Table 7.2 Various speckle shear interferometric configurations for slope contouring of 3-D objects

Optical configuration	Irradiance Distribution proportional to	Fringe Formation
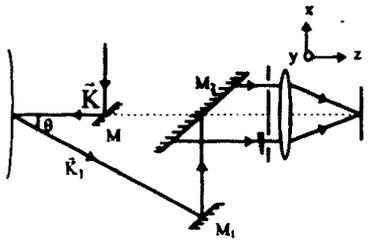	$c\{1+\cos[(\vec{K}_1-\vec{K})\cdot\frac{\partial\vec{L}}{\partial x}\Delta x_0]\}$	$\frac{\partial z}{\partial x}=\frac{m\lambda}{\Delta x_0\,\psi\sin\theta}$
	$c\{1+\cos[(\vec{K}_2-\vec{K})\cdot\frac{\partial\vec{L}}{\partial x}\Delta x_0+(\vec{K}_2-\vec{K}_1)\cdot\vec{L}]\}$	$\frac{\partial z}{\partial x}\Delta x_0+2z=\frac{m\lambda}{\psi\sin\theta}$
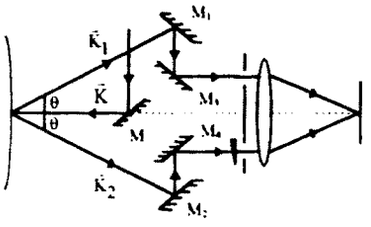	$c\{1+\cos[\frac{1}{2}(\vec{K}_1-\vec{K}_2)\cdot\frac{\partial\vec{L}}{\partial x}\Delta x_0]$ $+\cos[\frac{1}{2}(\vec{K}_1-\vec{K}_2)\cdot\frac{\partial\vec{L}}{\partial x}\Delta x_0+(\vec{K}_1-\vec{K}_2)\cdot\vec{L}]\}$	$\frac{\partial z}{\partial x}=\frac{m_1\lambda}{\Delta x_0\,\psi\sin\theta}$ $\frac{\partial z}{\partial x}\Delta x_0+2z=\frac{m_2\lambda}{\psi\sin\theta}$
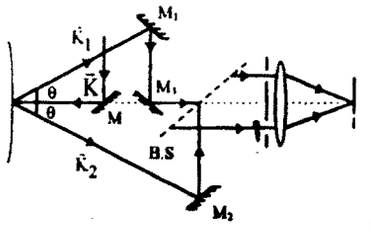	$c\{2+\cos[\frac{1}{2}(\vec{K}_4-\vec{K}_1)\cdot\frac{\partial\vec{L}}{\partial x}\Delta x_0$ $+(\vec{K}_4-\vec{K}_2)\cdot\frac{\partial\vec{L}}{\partial x}\Delta x_0+(\vec{K}_4-\vec{K}_3)\cdot\vec{L}]$ $\cos[\frac{1}{2}(\vec{K}_2-\vec{K}_1)\cdot\frac{\partial\vec{L}}{\partial x}\Delta x_0]$ $+\cos[\frac{1}{2}(\vec{K}_4-\vec{K}_1)\cdot\frac{\partial\vec{L}}{\partial x}\Delta x_0$ $+(\vec{K}_4-\vec{K}_2)\cdot\frac{\partial\vec{L}}{\partial x}\Delta x_0+(\vec{K}_4-\vec{K}_2)\cdot\vec{L}]$ $\cos[\frac{1}{2}(\vec{K}_2-\vec{K}_1)\cdot\frac{\partial\vec{L}}{\partial x}\Delta x_0+(\vec{K}_2-\vec{K}_1)\cdot\vec{L}]\}$	$\frac{\partial z}{\partial x}=\frac{m_1\lambda}{\Delta x_0\,\psi\sin\theta}$ $\frac{\partial z}{\partial x}\Delta x_0+2z=\frac{m_2\lambda}{\psi\sin\theta}$ $z=\frac{m_3\lambda}{2\,\psi\sin\alpha}$
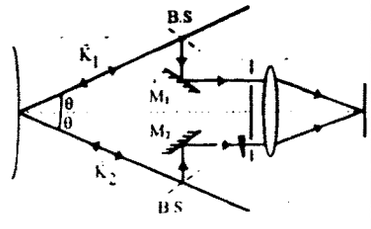	$c\{2+\cos[\frac{1}{2}(\vec{K}_1+\vec{K}_2)\cdot\frac{\partial\vec{L}}{\partial x}\Delta x_0+2\vec{K}_2\cdot\frac{\partial\vec{L}}{\partial x}\Delta x_0$ $+(\vec{K}_2-\vec{K}_1)\cdot\vec{L}][\cos[\frac{1}{2}(\vec{K}_2-\vec{K}_1)\cdot\frac{\partial\vec{L}}{\partial x}\Delta x_0]$ $+\cos[\frac{1}{2}(\vec{K}_2-\vec{K}_1)\cdot\frac{\partial\vec{L}}{\partial x}\Delta x_0+(\vec{K}_2-\vec{K}_1)\cdot\vec{L}]]\}$	$\frac{\partial z}{\partial x}=\frac{m_1\lambda}{\Delta x_0\,\psi\sin\theta}$ $\frac{\partial z}{\partial x}\Delta x_0+2z=\frac{m_2\lambda}{\psi\sin\theta}$

earlier method proposed by Sirohi and Krishna Mohan (1992). The detailed theory and experimental results are presented in Chapter 3.

In Chapter 4, the different configurations discussed in Chapter 2 have been implemented for contouring of 3-D objects. Contour fringes are generated by exposing the object twice on a holographic plate with a small tilt perpendicular to the plane of illumination between the exposures. The contour interval obtained earlier using this concept was in the range of 5–6 mm. However the configuration developed by us (Figure 2.7) yields for the first time a contour interval of 0.56 mm (564 μm) with fringes of nearly holographic quality. It was observed that decorrelation is very low as the beams are combined independently at the image plane via the two small apertures. Therefore this configuration can be used for industrial applications particularly for on-line production. The two-fold increase in sensitivity configuration presented in Section 2.6.1 is much more useful whereby even lesser contour intervals may be obtained.

In Chapter 5, various configurations have been given for slope change contouring of 3-D objects. Slope contours are generated based on the tilt in between exposures as discussed in Chapter 4 and by introducing a small shear in one of the waves at the image plane. All the configurations are in-plane displacement sensitive, and hence any out-of-plane displacement component or its derivative do not influence the fringe pattern but controls the contrast of the fringes. It is observed that single beam illumination or single beam observation do not provide the whole information of the object due to optical shadowing. This problem has been solved in the configurations employing two beams for illumination / observation, whereby even deep curved objects can be contoured. A configuration with a two-fold increase in sensitivity for slope change contouring is given and is backed up by experimental evidence for the first time. Here the scattered rays are observed from the same direction as that of the illumination rays with the

help of a beam splitter. It is worth noting that there is no necessity for the object to be coated with retro-reflective paint unlike in the in-plane displacement measurement.

It was thought that any configuration which is sensitive to in-plane displacement may be used for slope change contouring as explained earlier. However it has been observed and proved theoretically that the configuration shown in Figure 2.7 with the shearing element (wedge plate) in front of one of the apertures does not generate slope contours but only generates depth contours with a shift in its symmetry dependent upon the shear magnitude. Other merits and demerits of the proposed configurations are discussed in the concerned sections. The different configurations discussed in Chapter 5 for slope contouring are given in Table 7.2 with their intensity distributions and sensitivity.

Two simple optical configurations based on diffused reference beam have been developed for electronic speckle pattern interferometry. The reference beam is generated at the CCD plane by illuminating a tiny diffuser which is mounted on the CCD camera lens mount with a portion of object beam. These configurations have several merits over the conventional ones, such as simplicity, cost, alignment and area of observation etc. The experimental results and advantages of these configurations are discussed in Chapter 6.

7.2 CONCLUSION

In this thesis attempts have been made to develop some new optical techniques for deformation measurements and contouring in speckle interferometry. The main developments of the investigation are:

1. Development of a speckle interferometric configuration for the measurement of in-plane displacement components of a deformation vector by simultaneously implementing the concepts of both Leendertz's and Duffy's techniques.
2. Development of a novel image plane speckle interferometric configuration for in-plane displacement measurement with unit contrast fringes.
3. Development of an in-line speckle interferometer for in-plane displacement measurement.
4. A new theoretical concept has been derived for the measurement of in-plane displacement component with a two-fold increase in sensitivity.
5. Development of a multi-aperture speckle interferomtric configuration for the simultaneous measurement of in-plane and out-of-plane displacement components.
6. Among the configurations used in contouring image plane speckle interferometric configurations exhibited higher sensitivity.
7. Among the configurations studied for slope contouring, the configurations with either two beam illumination or two beam observation were found to be the right candidates enabling even deeply curved objects to be contoured.
8. Two simple configurations for ESPI based on diffused reference beam have been devised.
9. The presently developed method also attempts to obtain a two-fold increase in sensitivity for contouring and slope change contouring of 3-D objects.

7.3 SUGGESTIONS FOR FUTURE WORK

1. The study can be further extended to strain analysis and displacement derivative measurements with some modifications in their respective configurations.
2. The decorrelation factor, which limits the maximum measurable sensitivity of the configurations, is useful for studying the decorrelation factor associated with the image plane speckle interferometric configuration shown in Figure 2.7 as this configuration exhibited interesting features.
3. One can develop new time-saving and cost-effective methods for the simultaneous measurement of displacement components and their derivatives etc.
4. This study can also be utilized for various specific applications such as thermal distortion measurements, strain analysis etc. by incorporating phase shifting techniques.
5. Although several commercial ESPI systems for measuring out-of-plane displacements are available, only very few systems for measuring in-plane displacement exist. Therefore it is of great importance to develop a commercial unit, with proper instrumentation, for the configuration shown in Figure 2.11 as it allows electronic processing.